

APPENDIX C – GEANT4 SIMULATION CODE

Detection configurations optimum for the ELI-NP experimental conditions created by the LCS γ -ray beam time structure were investigated using a complex end-to-end simulation code developed using the Geant4 toolkit for the simulation of the passage of particles through matter[All06,Ag03]. A realistic model of laser photon – relativistic electron interaction was implemented in the code for the investigation of the energy and intensity γ -ray beam profile along with γ -ray beam polarization type and degree. The simulation code was tested against experimental data taken at the LCS γ -ray beam facility NewSUBARU and it successfully reproduced both γ -ray energy and intensity profiles. Ideal radiation sources are also implemented in the code for increased computing speed necessary for detection efficiency and background studies. The ELI-NP experimental hall configuration was also implemented in the code, including the γ -ray collimator and beam dump. The experimental setups proposed by the GANT workgroup were implemented in a flexible manner, allowing the investigation of various geometries and combinations of detectors and shielding layers.

C.1 RADIATION SOURCES

C.1.1 LASER COMPTON SCATTERING GAMMA-RAY SOURCE

The LCS γ -ray source implemented in the Geant4 code provides the energy, the direction and the state of polarization of a γ -rays generated by the interaction between a laser photon and an electron beam. Our simulation code of laser photon – relativistic electron interaction considerably improves previous models, such as EGS4, because it generates Compton scattering events at arbitrary angles, not only ideal head – on collisions. The collision parameters are generated considering the emittance of the electron beam and the spatial distribution of the laser beam. The simulation code is briefly described in the following section.

Electron and laser beam characterization

Two coordinate systems are defined to describe the electron and laser beams. The electron beam coordinate system (x , y , z) coincides with the global coordinate system in which the electron beam is moving along the z axis towards positive values. The (x_l , y_l , z_l) system is the laser beam coordinate system in which the laser beam is propagated along the z_l axis towards negative values, at polar angles θ and φ relative to electron beam axis. The coordinate systems (x , y , z) and (x_l , y_l , z_l) are shifted on the z axis with Δz , the distance between the focal points of the laser and electron beams. This very general situation is represented in Figure C.1.a.

Both the electron and the laser beam from NewSUBARU have a pulsed time structure but they are unsynchronized in time and space. Therefore the laser photon – electron interaction takes place anywhere along the 20 meters long electron beam axis with highest probability inside the region between the two waist point of the electron and of the laser beam. This

situation is represented in Figure C.1.b, where the two beams are sent head on against each other and the laser beam axis coincides with the electron beam axis.

The laser and electron beam pulses are synchronized in time and space at ELI-NP, therefore the interaction point is very well-defined within $\sim 1\text{mm}$. This configuration is represented in Figure C.1.c, where the interaction region is determined by the spatial length of one electron micro-bunch. A polar angle $\theta = 7.5^\circ$ between the laser and the electron beam axis is implemented in the code for this collision configuration.

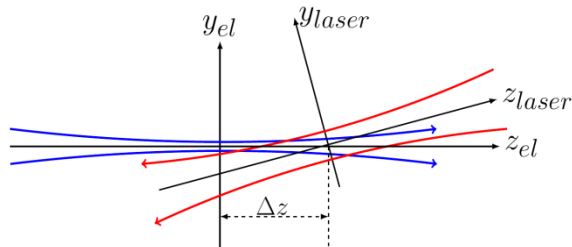


Figure C.1.a Schematic representation of laser and electron beams – general case. The electron and the laser beam have different propagation axis. There is a Δz distance along the electron beam axis between the focal points of the electron and laser beams. Both the electron and laser beam are continuously distributed.

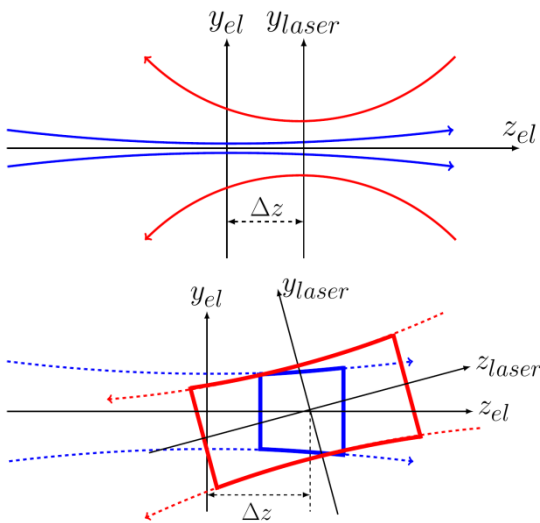


Figure C.1.b Schematic representation of laser and electron beams at NewSUBARU. The electron and laser beams are sent head on against each other, thus the electron beam axis coincides with the laser beam axis.

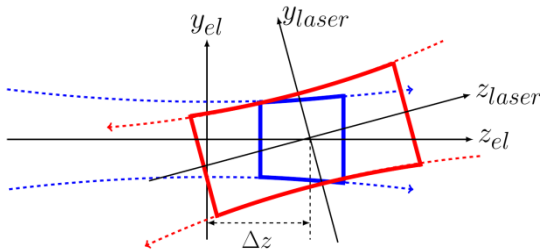


Figure C.1.c Schematic representation of laser and electron beams at ELI-NP. There is a $\theta = 7^\circ$ between the two axis. Both the laser and the electron beam have a pulsed structure. The interaction takes place in a well-defined point along the electron beam axis.

Regardless of the interaction region length, inside it both the electron and the laser beams are considered continuously distributed. In the case of drift spaces, where particles move freely through the beam line with no external fields applied, if the particle coordinates and the Twiss parameters are known in a single position, they can be expressed in any point along the beam line. The electron beams are implemented in the Geant4 code considering an ideal Gaussian phase-space distribution fully characterized by the electron beam transverse size at focal point and the electron beam normalized emittance.

The laser photon beam is implemented as a Gaussian beam fully characterized by its wavelength, beam waist and quality factor.

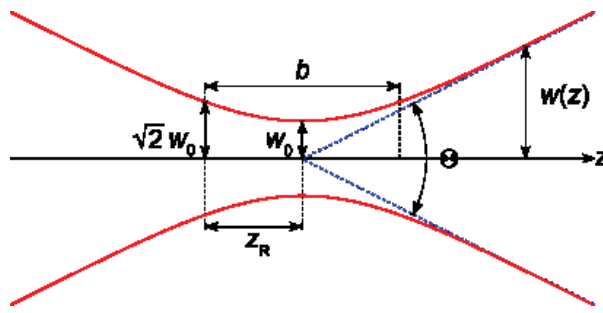


Figure C.2 Schematic view of laser beam transverse beam size (hyperbolic dependence along the beam axis), where w_0 is the beam size at focal point, and $z_R = b/2$ represents the Rayleigh length.

Generate interaction point

The interaction between laser photons and electrons can take place anywhere along the z axis inside the interaction region defined by the user, which in the case of ELI-NP is a 400 μm long micro bunch and at NewSUBARU is a 20 m long straight beam line. For a given z_i point along the z axis, the interaction point coordinates in the transverse plane are generated following the transverse electron beam spatial distribution described by the Twiss parameters. The share of one event is equal to the laser photon density at the interaction point $I_p(x_l(z_l), y_l(z_l), z_l)$.

Generate laser and electron Lorentz vectors

The electron momentum projections on transverse plane axis are obtained using the Twiss parameters for the generated (x, y, z) interaction point. The momentum direction of the laser photon at the collision point (x_l, y_l, z_l) in the laser beam coordinate system can be calculated in the view of electromagnetic wave of the Gaussian laser beam.

Both the electron and the laser photon energy values are generated according to Gaussian distributions with a E_e , respectively e_L , mean and given deviations, where E_e is the electron beam energy and e_L is the laser photon energy corresponding to the laser central wavelength. Both at ELI-NP and at NewSUBARU, Nd:YVO₄ laser beams are used, with 1064 nm central wavelength 0.05 % bandwidth.

Generate laser photon polarization state

Laser beams more than 99% linearly polarized and unpolarized electron beams will be employed at ELI-NP for production of γ -ray beams. Therefore the polarization state and degree of the laser beam was fully implemented in the Geant4 simulation code using the formalism of the Stokes parameters defined in terms of the density matrix (or statistical matrix). The theory of the Stokes parameters is briefly organized in [McM54].

Generate energy and direction of scattered photon

For convenience, the sampling probability for generating gamma-ray photon parameters is calculated in the electron-rest frame coordinate system (x_e, y_e, z_e) in which the electron is at rest and the laser photon is propagated along the z_e axis direction. For this, the global coordinate system is rotated to align the electron on the z axis. A Lorentz transformation with

$\beta = v_e / c$ is applied to obtain the electron-rest frame coordinate system (x_e , y_e , z_e). The electron-rest frame is afterwards rotated to align the laser photon on the z_e axis direction. Thus, the Compton interaction differential cross section is computed for a simple head-on collision with the electron at rest using the Klein Nishina distribution. This method was taken from the PhD thesis of Dr. C. Sun [Sun09].

Lorentz transformation with $\beta = v_e / c$ is performed in z_e direction on the scattered photon's quadrivector to transform the electron rest frame coordinate system into the laboratory frame electron beam coordinate system. The electron energy E_γ in the laboratory frame coordinate system is obtained. The new γ -ray photon quadrivector is rotated according to the initial electron direction to obtain the direction of the γ -ray photon.

An example of the input file which contains the laser and electron beam parameters is given in Table C.2:

Input value	Unit	Comments
250	GW	Laser power
400	A	Electron beam current
750	MeV	Electron beam central energy
0.04	%	Electron beam central energy spread
532	nm	Laser beam wavelength
0.05	%	Laser beam energy spread
0.025	mm	Laser beam focal spot size (sigma)
0	mm	Laser – electron beam waist displacement – x axis
0	mm	Laser – electron beam waist displacement – y axis
0	mm	Laser – electron beam waist displacement – z axis
0	mm	Electron beam waist position on x axis of the experimental hall coordinates system
0	mm	Electron beam waist position on y axis of the experimental hall coordinates system
-0.004	m	Upstream limit of laser photon – electron interaction area range
+0.004	m	Downstream limit of laser photon – electron interaction area range
0.03	mm	Electron beam focal spot size (sigma) – horizontal axis
2.00E-004	mm×rad	Electron beam normalized emittance – horizontal axis
0.03	mm	Electron beam focal spot size (sigma) – vertical axis
2.00E-004	mm×rad	Electron beam normalized emittance – vertical axis
7.5	deg	Polar angle θ between laser beam and electron beam axis
-10.0	deg	Polar angle φ between laser beam and electron beam axis. If the input value is negative, all 32 incident directions given by the recirculating system are considered.
90.0	deg	Laser beam linear polarization angle τ .
100	%	Laser beam linear polarization percentage
0	%	Laser beam circular polarization percentage
1	–	Switch: 1 = consider electron beam input parameters listed above. 0 = consider ideal electron beam with no transverse components of electron momentum and constant electron energy equal to the electron beam central energy.
1	–	Switch: 1 = consider laser beam input parameters listed above.

		0 = consider ideal electron beam with no transverse components of laser photon momentum in the laser beam coordinate system and constant photon energy equal to the laser beam central energy.
--	--	--

Table C.2 Electron and laser beam Geant4 code input parameters. The each input parameters is explained in Column 3. The values given as example in Column 1 represent the ELI-NP expected parameters.

Geant4 LCS γ -ray source code validation against existing LCS γ -ray source code EGS4

A comparison was made between the results of the EGS4 code and the Geant4 code for identical input parameters and for the same number of simulated events. Only head-on collisions were generated by the Geant4 source. The same effective beam size of 1.8 mm was considered for both sources. In the case of the Geant4 code results, the share of each event is equal to 1, and not to the laser photon density as described above. A 710.59 MeV electron beam of 0.04 % energy resolution and a Nd:YVO₄ laser were considered. The incident polar angles were restricted to 0 degrees for both the electron and the laser photon. The collimated spectra incident on a cylindrical 3.5" × 4" crystal placed in beam, aligned with the electron beam axis at 25 meters from the focal point of the electron beam, are represented in in Figure C.3. The spectra obtained with the two methods are identical and have the same number of counts.

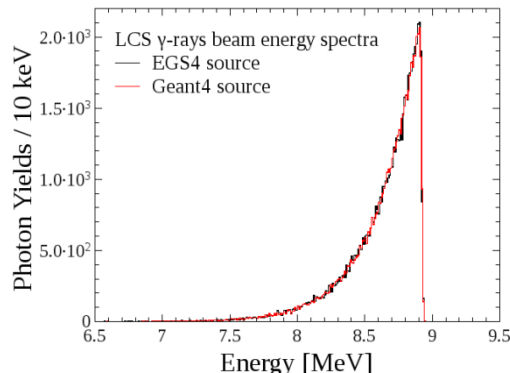


Figure C.3 Incident LCS γ -ray on crystal after collimation. Two simulations codes were used: the head-on gamma source implemented in EGS4 (black) and the Geant4 code which takes into consideration the electron and laser phasespaces (red). In this example only head-on collisions were considered for both simulations, in order to test the results similarity.

Geant4 LCS γ -ray source code validation against NewSUBARU experimental data

The γ -ray beams are produced at NewSUBARU by the collision between either a Nd:YVO₄ laser in the first harmonic or a CO₂ laser in the first harmonic with electron beams of highly precise energy between 0.5 GeV to 1.5 GeV. The NewSUBARU electron beam central energy resolution is of 0.04 % and it was recently calibrated between 550 and 974 MeV with accuracy of the order of 10⁻⁵ [Uts14]. Therefore, as will be the case of ELI-NP, the γ -ray beams have a precisely defined, sharp high energy front, as can be seen in Figure 4.2.3. After collimation, the γ -ray beam presents a low energy tail with a small energy width of ~1.2 to 1.6 % in FWHM values, depending on collimator thickness and aperture.

A complex collimation system consisting of four main collimators is employed at NewSUBARU. A large aperture (2 cm) first collimation stage consisting in a water cooled Copper collimator placed near the interaction point is used for protecting the electron pipe and from high flux γ -ray beams. A second collimator stage of large aperture (5 cm) consisting in a 30 cm thick lead block placed at approximately 13 meters from the interaction

point is used for absorbing γ -rays scattered at large angles. The fine tuning collimation system consists of two 10 cm thick lead blocks (C1 and C2 collimators) of variable apertures (1 to 6 mm). The entire collimation system was implemented in our Geant4 code.

The energy profile of γ -ray beams with maximum energies between 6 and 13 MeV produced using the 1.064 μm wavelength Nd:YVO₄ laser were recorded with a large volume cylindrical 3.5" \times 4" LaBr₃:Ce, BrilLanCe380 89S102/3.5, Saint Gobain detector. Gamma ray beams with lower maximum energies, up to 3 MeV, produced using the 10.59 μm wavelength CO₂ laser were recorded with a 45% relative efficiency coaxial HPGe detector. Experimental energy spectra of LCS γ -ray beams and Geant4 simulations of detector response and of energy spectra of collimated γ -ray beams incident on the monitoring detector are displayed in Figures C.4.a–d and C.5. Geant4 simulations reproduce the energy spectra of γ -ray beams produced using both types of lasers employing different collimation configurations and recorded both types of detectors. Also, the relative intensity of the LCS γ -ray beam using different collimation configurations is also very well reproduced by the simulations, as can be observed in Figure 4.2.5.

Figure C.4.a shows a typical spectrum of the LCS γ -ray beam recorded with the LaBr₃:Ce detector (solid line) along with the GEANT4 simulations of the detector response function (dotted line) and the incident γ -ray beam (gray line). The spectra are renormalized for better visualization. The experimental response function was obtained without the C1 collimator. One can see a broad low-energy bump around 3 MeV in the response function. This bump is characteristic of spectra obtained without the C1 collimator, which was confirmed experimentally under the presence and absence of the C1 collimator. The bump corresponds to the laser photons Compton-scattered around 0° with large cross sections in the rest frame of electrons which, after a Lorentz boost by relativistic electrons in the laboratory frame, punched through the 10 cm C2 collimator. The punch-through component is seen in the low-energy region of the incident γ -ray spectrum.

Figure C.4.b shows typical spectra of the LCS γ -ray beams recorded with the LaBr₃:Ce detector (solid lines) along with the GEANT4 simulations of the detector response function (dotted lines) and the incident γ -ray beam (gray lines). The experimental response functions were obtained by using the double collimation system with a C1 collimator of 6 mm aperture. The low-energy component is absent in the response function obtained with the double collimation system, which confines the scattering angles into a narrower cone along the electron beam axis with a total thickness of 20 cm. The experimental response functions are well reproduced by the GEANT4 simulation.

Beam intensity results of GEANT4 simulations have been tested against experimental data taken at NewSUBARU during a study on the effects of the collimation system transverse misalignments relative to the electron beam axis. Electron beams with constant energy of 982.43 MeV and \sim 300 mA current and a 35 mW Nd:YVO₄ laser operated in continuous mode were used to produce γ -ray beams. The energy spectra and the intensity of the LCS beam were recorded with the 3.5" \times 4" LaBr₃:Ce detector. A double collimation with a C1 collimator of 3 mm aperture and a C2 collimator of 2 mm aperture was employed.

Figure C.5 shows experimental and simulated LCS γ -ray beam energy spectra recorded for various C2 collimator vertical misalignments having the C1 collimator aligned with the electron beam axis. Effects on the intensity and energy spectra of the γ -ray beam are correctly

reproduced by the Geant4 simulation. The experimental beam intensity is reproduced by the simulations by a constant factor.

Characterization of ELI-NP LCS γ -ray source

A complete characterization of the ELI-NP γ -ray source can be carried out using the Geant4 simulation code validated against experimental data.

The simulation code can provide the:

- γ -ray beam energy spectra incident on a monitor detector;
- transverse energy and intensity beam profile;
- type and degree of polarization,

by placing a monitor target anywhere along the beam axis.

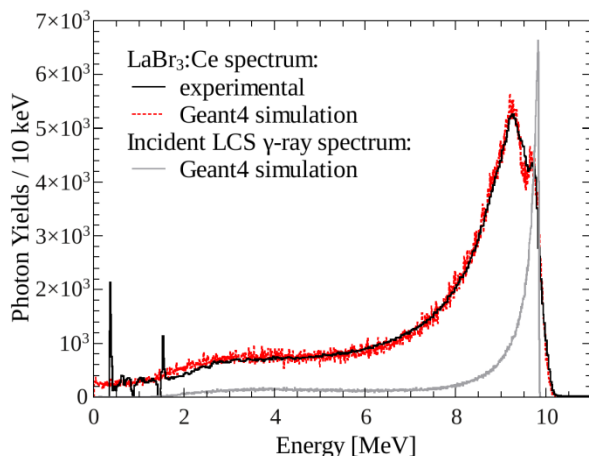


Figure C.4.a Typical spectra of γ -ray beams recorded with the LaBr₃:Ce detector (solid lines) and the simulations of the response function (dotted lines) and of the incident γ -ray beam (gray lines). A double collimation with a C1 collimator of 6-mm aperture and a C2 collimator of 2-mm aperture was employed. The 6.5 MeV, 10.0 MeV and 13.0 MeV maximum energy γ -ray beams are produced using a 1064 nm wavelength Nd:YVO₄ laser and electron beams of 607.03 MeV, 753.77 MeV and 860.84 MeV, respectively.

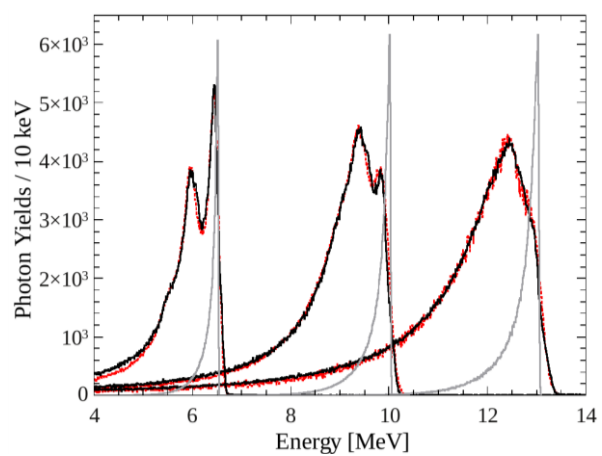


Figure C.4.b A typical spectrum of the γ -ray beam recorded with the LaBr₃:Ce detector (solid line) and the simulations of the response function (dotted line) and of the incident γ -ray beam (gray line). A single collimation with a C2 collimator of 2-mm aperture was used. The 9.82 MeV maximum energy γ -ray beam is produced using a 1064 nm wavelength Nd:YVO₄ laser and an electron beam of 746.74 MeV.

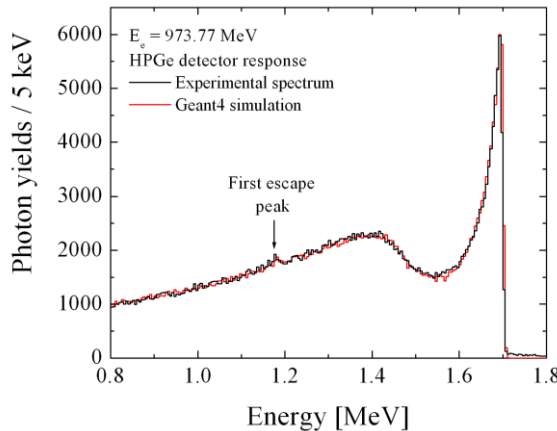


Figure C.4.c A typical spectrum of the γ -ray beam recorded with the HPGe detector (black) and the simulation of the response function (red). A double collimation with a C1 collimator of 3 mm aperture and a C2 collimator of 1 mm aperture was employed. The 1.6974 MeV maximum energy γ -ray beam is produced using a 10.59 μm wavelength CO₂ laser and an electron beam of 973.77 MeV.

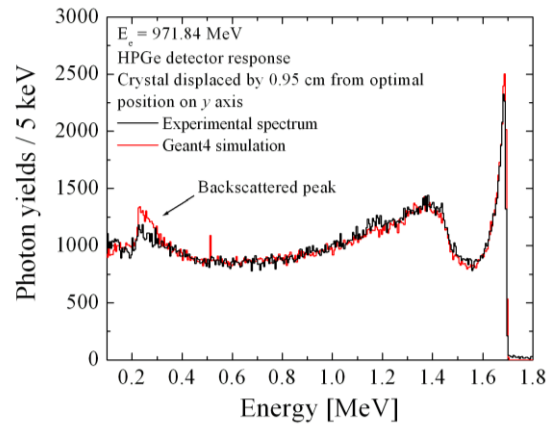


Figure C.4.d Same as Figure 4.2.4.c but a 971.84 MeV electron beam is used to generate a 1.6907 MeV maximum energy γ -ray beam. In this case the HPGe crystal was displaced by 0.95 cm from the optimal position on the y axis. This displacement was determined by best reproducing the experimental spectrum with the Geant4 simulations.

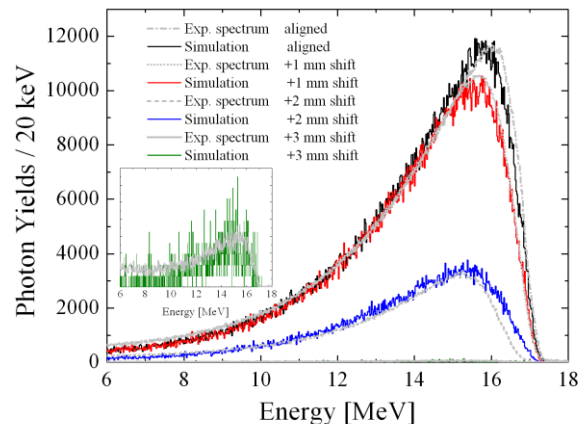
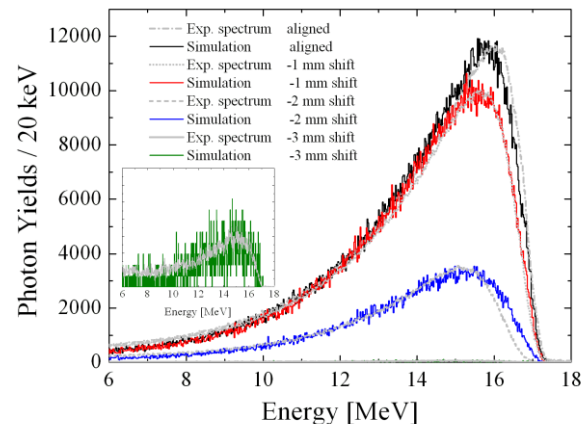


Figure C.5 Experimental and simulated LCS γ -ray beam energy spectra recorded for various C2 collimator vertical misalignments having the C1 collimator aligned with the electron beam axis. The spectra were recorded with a cylindrical 3.5" \times 4" LaBr₃:Ce detector. The intensity of the simulated spectra differ from the experimental one only by a constant factor. The experimental energy profile is also well reproduced by the simulations.



Characterization of ELI-NP LCS γ -ray source – Before collimation process

The γ -ray beam characteristics were simulated before collimation employing the ELI-NP expected electron and laser beam parameters. A thin 2 cm diameter Lead target was placed at 2.3 meters from the high energy laser – electron interaction point, before the γ -ray collimator. Gamma ray beams were produced employing ELI-NP expected electron and laser beam characteristics:

- Laser photon – electron interaction area length: 8 mm along the electron beam axis;
- Polar angle $\theta = 7.5$ deg between laser and electron beam axis;
- Electron beam:
 - energy $E_{el} = 750$ MeV
 - normalized emittance: $\epsilon_{n-x,y} = \epsilon_{n-x} = \epsilon_{n-y} = 0.2$ mm×mrad;
 - focal spot size: $\sigma_{el} = \sigma_{el-x} = \sigma_{el-y} = 15$ μm ;
 - central energy spread: $\Delta E_{el} = 0.04$ %;
- Laser beam:
 - wavelength: $\lambda = 532$ nm;
 - central energy spread: $\Delta E_{laser\ photon} = 0.05$ %;
 - focal spot size: $w_0 = 25$ μm .
- Gamma ray beam:
 - maximum energy: $E_\gamma^{max} = 19.557$ MeV

	A1	B1	C1	D1	E1	F1	G1
Linear polarization angle [deg]	90	0	90	90	20	-	20
Linear polarization [%]	100	100	100	95	100	0	50
Circular polarization [%]	0	0	0	0	0	100	30
Laser beam polar angle ϕ [deg]	*	*	45	*	*	*	*

Table C.3 Laser photon polarization state, degree of polarization and linear polarization angle used as input parameters for Geant4 simulations on LCS γ -ray beam energy and intensity profiles and on γ -ray beam polarization characteristics.

The gamma ray beam characteristics were investigated by employing different types and degrees of laser polarization, as listed in Table C.2. Seven different scenarios were investigated, using both linear and circular polarized laser beams. For each scenario, the laser beam linear polarization degree and angle, the circular polarization degree and the laser incident polar angles ϕ between the laser and the electron beam axes.

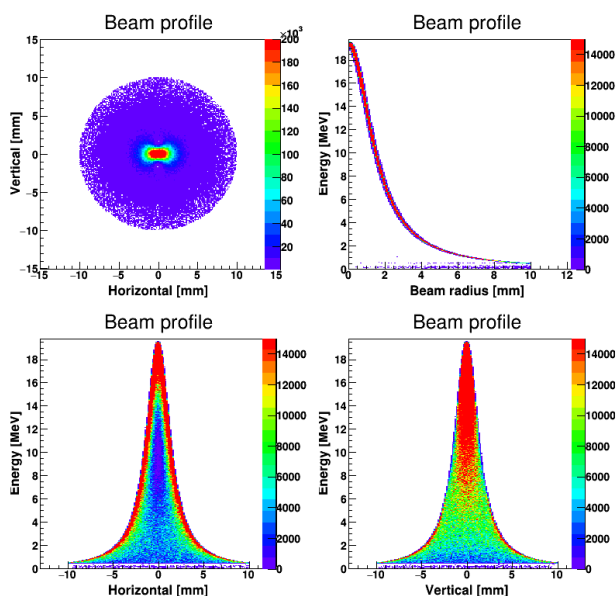


Figure C.6.a Geant4 simulation of the transverse energy profile of a 19.557 MeV maximum energy γ -ray beam produced using a 100% linearly polarized laser beam with polarization angle $\tau = 90^\circ$, corresponding to the A1 scenario listed in Table C.3. The energy profile was investigated at 2.3 meters from the interaction point.

Upper left: γ -ray beam intensity profile.

Upper right: γ -ray beam energy distribution versus beam radius.

Lower left: γ -ray beam energy distribution on the horizontal beam axis.

Lower right: γ -ray beam energy distribution on the vertical beam axis.

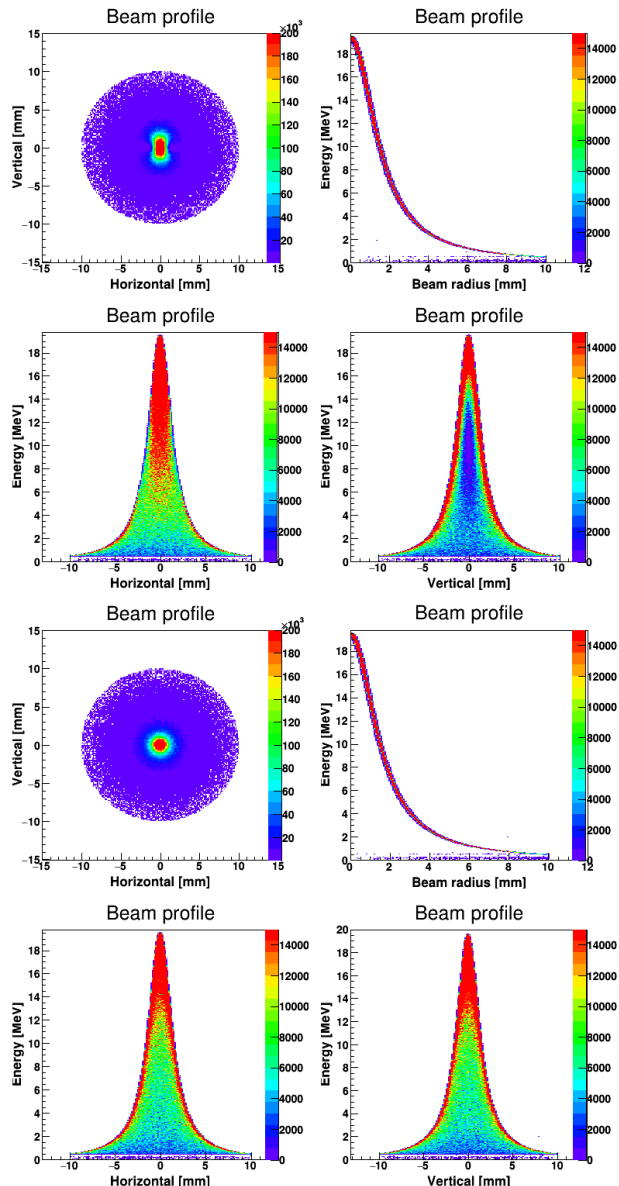


Figure C.6.b Same as Figure C.6.a but for the B1 configuration described in Table C.3. The laser beam used for γ -ray beam production is 100% linearly polarized laser photons with polarization angle $\tau = 0^\circ$.

Figure C.6.c Same as Figure C.6.a but for the F1 configuration described in Table C.3. The laser beam used for γ -ray beam production is 100% circularly polarized laser photons.

Transverse energy profiles of 19.557 MeV maximum energy γ -ray beams provided by the Geant4 laser photon – electron interaction code are shown in Figure C.6. The electron and laser phase-space and energy input parameters were listed above. The laser photon polarization input parameters correspond to the A1, B1 and F1 scenarios listed in Table C.3, thus we investigated the results of the Geant4 simulations for three states of purely polarized laser beams: totally linearly polarized laser photons on with polarization angles $\tau_1 = 90^\circ$ and $\tau_2 = 0^\circ$, shown in Figure C.6.a and C.6.b respectively, and one totally circularly polarized laser photons, shown in Figure C.6.c.

The average energy and the intensity of the γ -ray beam as a function of the γ -ray beam radius obtained employing a 100% linearly polarized laser photon beam are represented in Figure C.7.

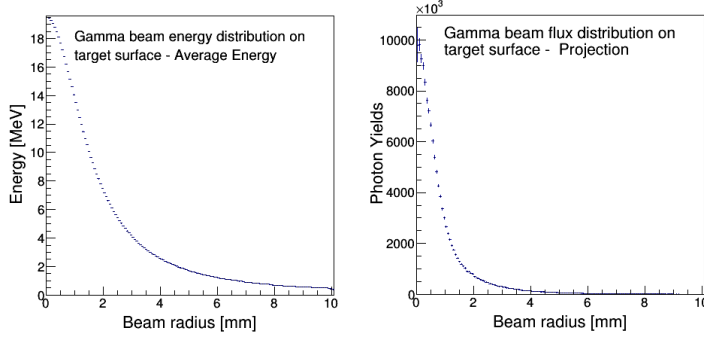


Figure C.7 Average energy of γ -ray beam versus γ -ray beam radius (left) and intensity of γ -ray beam versus γ -ray beam radius. The results are obtained using the Geant4 simulation code for the A1 configuration laser polarization input parameters listed in Table C.3. A 100% linearly polarized laser photon beam with polarization angle $\tau = 90^\circ$ was employed.

The following histograms provided by the Geant4 code:

- electron beam transverse intensity distribution integrated along the entire length of the interaction area;
- interaction point transverse intensity distribution obtained by the convolution of the electron and laser beams spatial distributions;
- electron beam vertical and horizontal phase-space distributions in the interaction point.
- transverse laser beam intensity profiles

that characterize a γ -ray beams obtained by employing a 100% linearly polarized laser photon beam having:

- all 32 values of the polar angle φ given by the laser beam recirculator;
- the polar angle $\varphi = 45^\circ$,

are represented in Figures C.8.a,C.9.a and C.8.b,C.9.b, respectively.

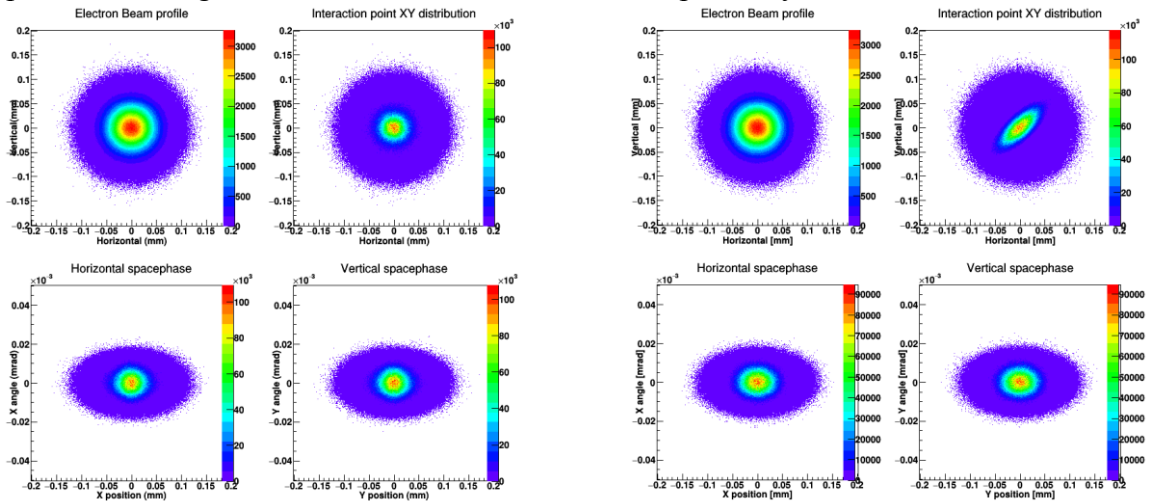


Figure C.8.a Transverse electron beam intensity profile (upper left), Interaction point transverse intensity distribution (upper right), Horizontal (lower left) and vertical (lower right) phase-space of electrons in the interaction point. Geant4 simulations employing a 100% linearly polarized laser beam with polarization angle $\tau = 90^\circ$ (A1 scenario, see Table 4.2.3) and all the 32 incident polarization angles φ given by the laser recirculator.

Figure C.8.b Same as Figure 4.2.8.a, but employing a 100% linearly polarized laser beam with polarization angle $\tau = 90^\circ$ (C1 scenario, see Table 4.2.3) and only one value of the incident polar angle $\varphi = 45^\circ$.

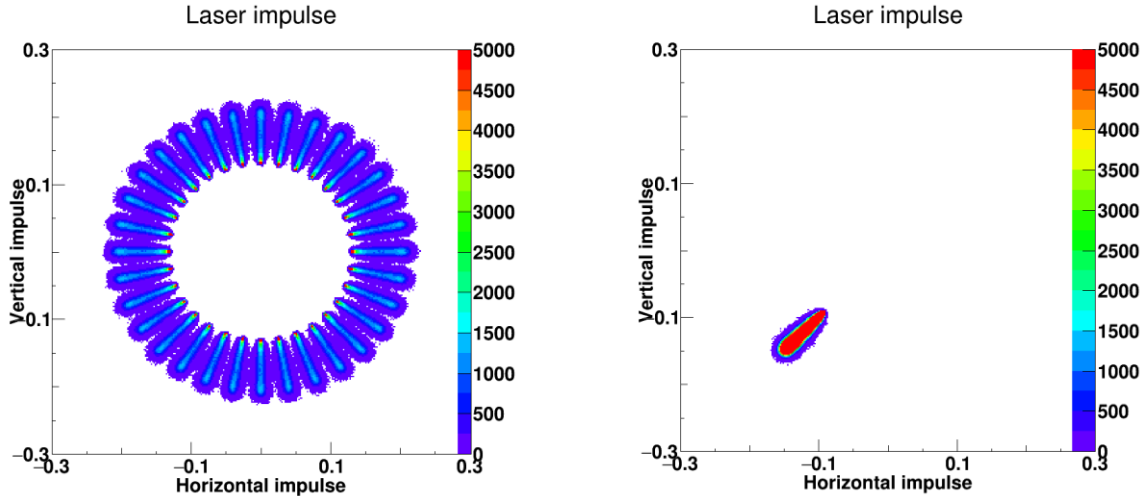


Figure C.9.a Transverse laser beam impulse intensity profile. Geant4 simulations employing a 100% linearly polarized laser beam with polarization angle $\tau = 90^\circ$ (A1 scenario, see Table C.3) and all the 32 incident polarization angles φ given by the laser recirculator.

Figure C.9.b Same as Figure C.9.a, but employing a 100% linearly polarized laser beam with polarization angle $\tau = 90^\circ$ (C1 scenario, see Table C.3) and only one value of the incident polar angle $\varphi = 45^\circ$.

The distributions of the γ -ray photons Stokes parameters and polarization angle as functions of the γ -ray beam energy were also provided for five different cases of types, degrees and angles of laser polarization:

- 100% linearly polarized, $\tau = 90^\circ$, see Figures C.10.a and C.11.a;
- 95% linearly polarized, $\tau = 90^\circ$, see Figures C.10.b and C.11.b;
- 100% linearly polarized, $\tau = 20^\circ$, see Figures C.10.c and C.11.c;
- 100% linearly polarized, $\tau = 0^\circ$, see Figures C.10.d and C.11.d;
- 100% circularly polarized, see Figures C.10.e and C.11.e.

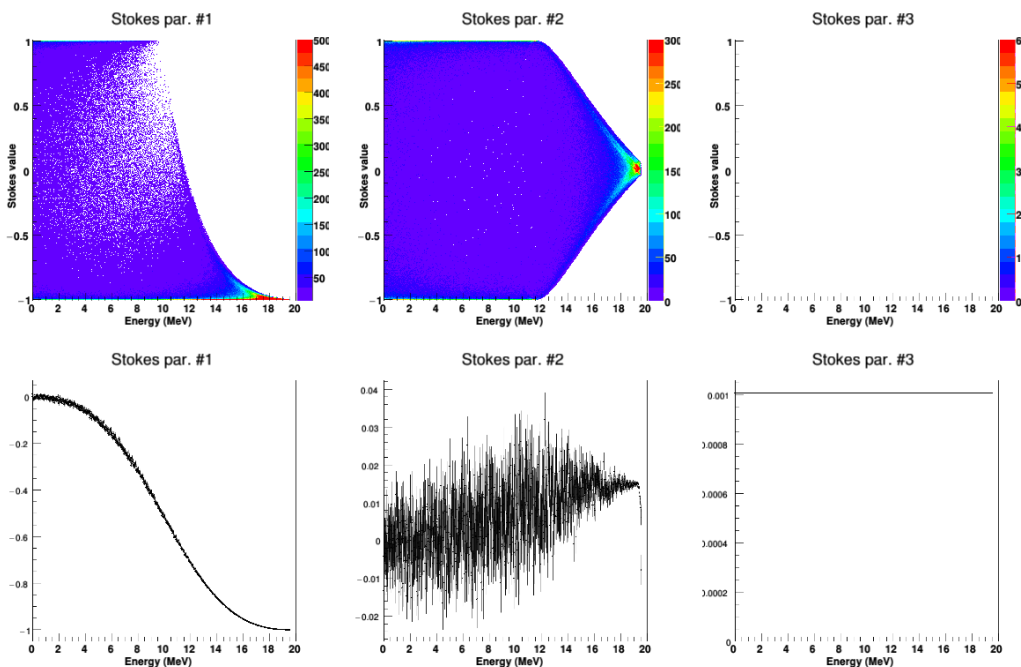


Figure C.10.a Geant4 simulation of distribution of γ -ray beam Stokes parameters versus energy.

The simulation was produced employing a 100% linearly polarized laser beam with polarization angle $\tau = 90^\circ$, corresponding to the A1 scenario described in Table C.3.

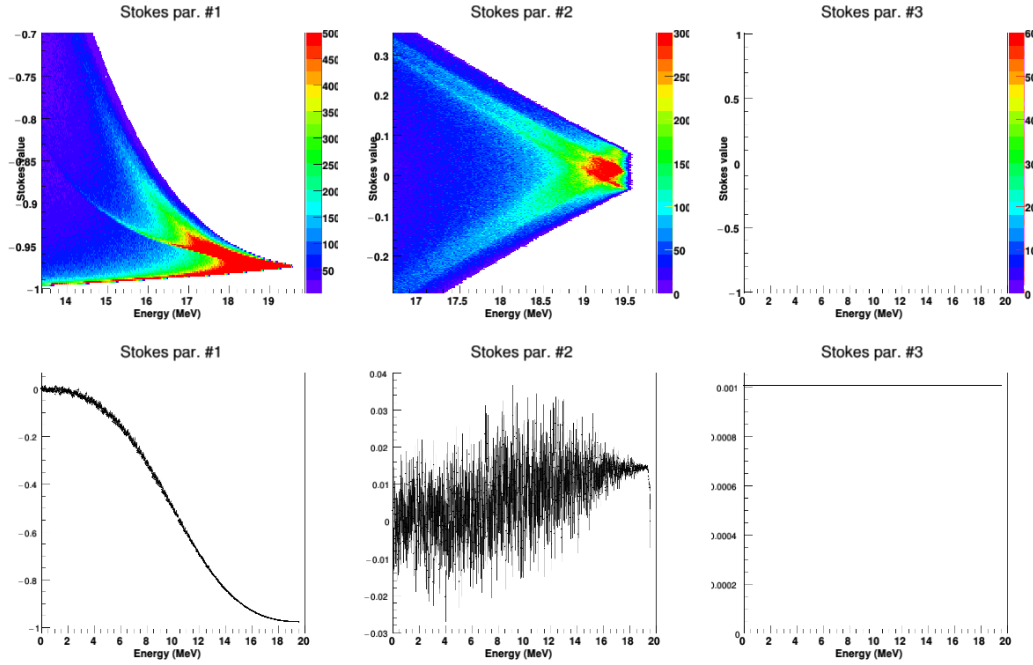


Figure C.10.b Same as Figure C.10.a but for a 95% linearly polarized laser beam with polarization angle $\tau = 90^\circ$, corresponding to the D1 scenario described in Table C.3.

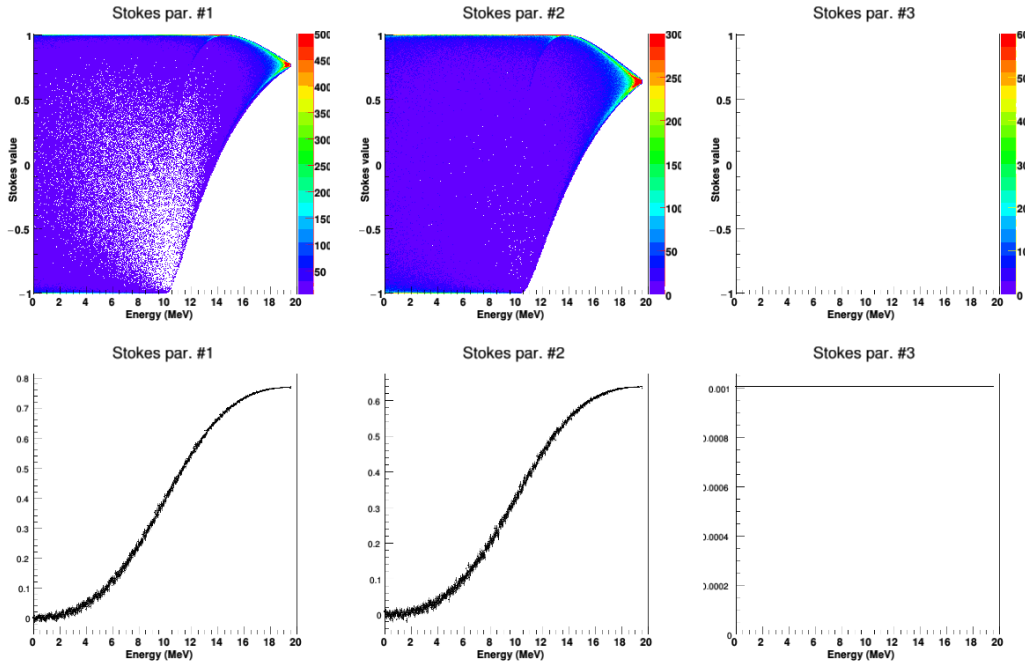


Figure C.10.c Same as Figure C.10.a but for a 100% linearly polarized laser beam with polarization angle $\tau = 20^\circ$, corresponding to the E1 scenario described in Table C.3.

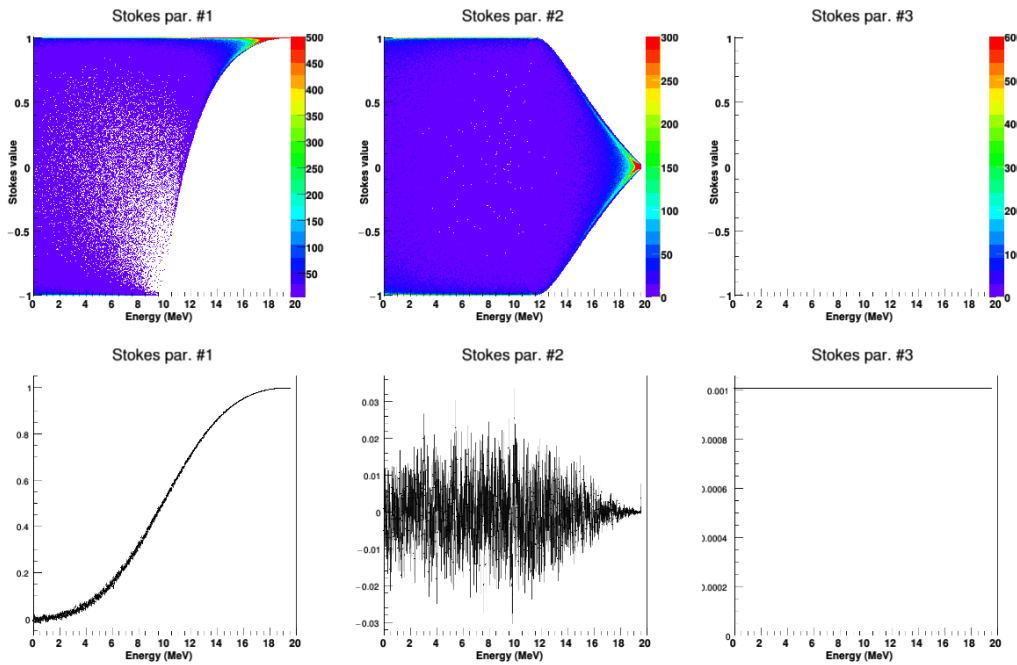


Figure C.10.d Same as Figure C.10.a but for a 100% linearly polarized laser beam with polarization angle $\tau = 0^\circ$, corresponding to the B1 scenario described in Table C.3.

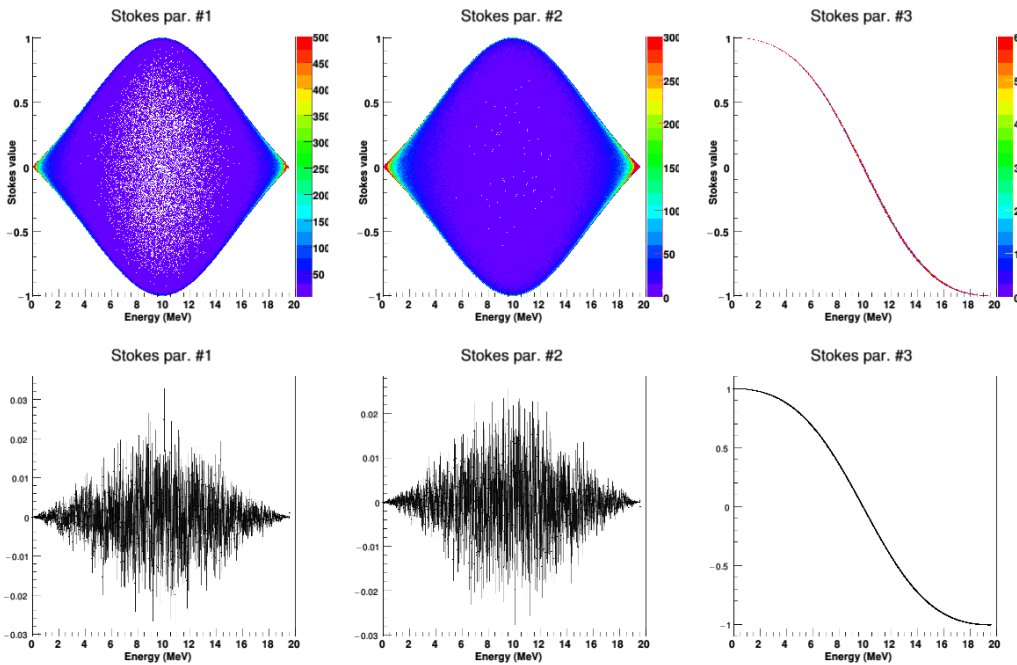


Figure C.10.e Same as Figure C.10.a but for a 100% circularly polarized laser, corresponding to the F1 scenario described in Table C.3.

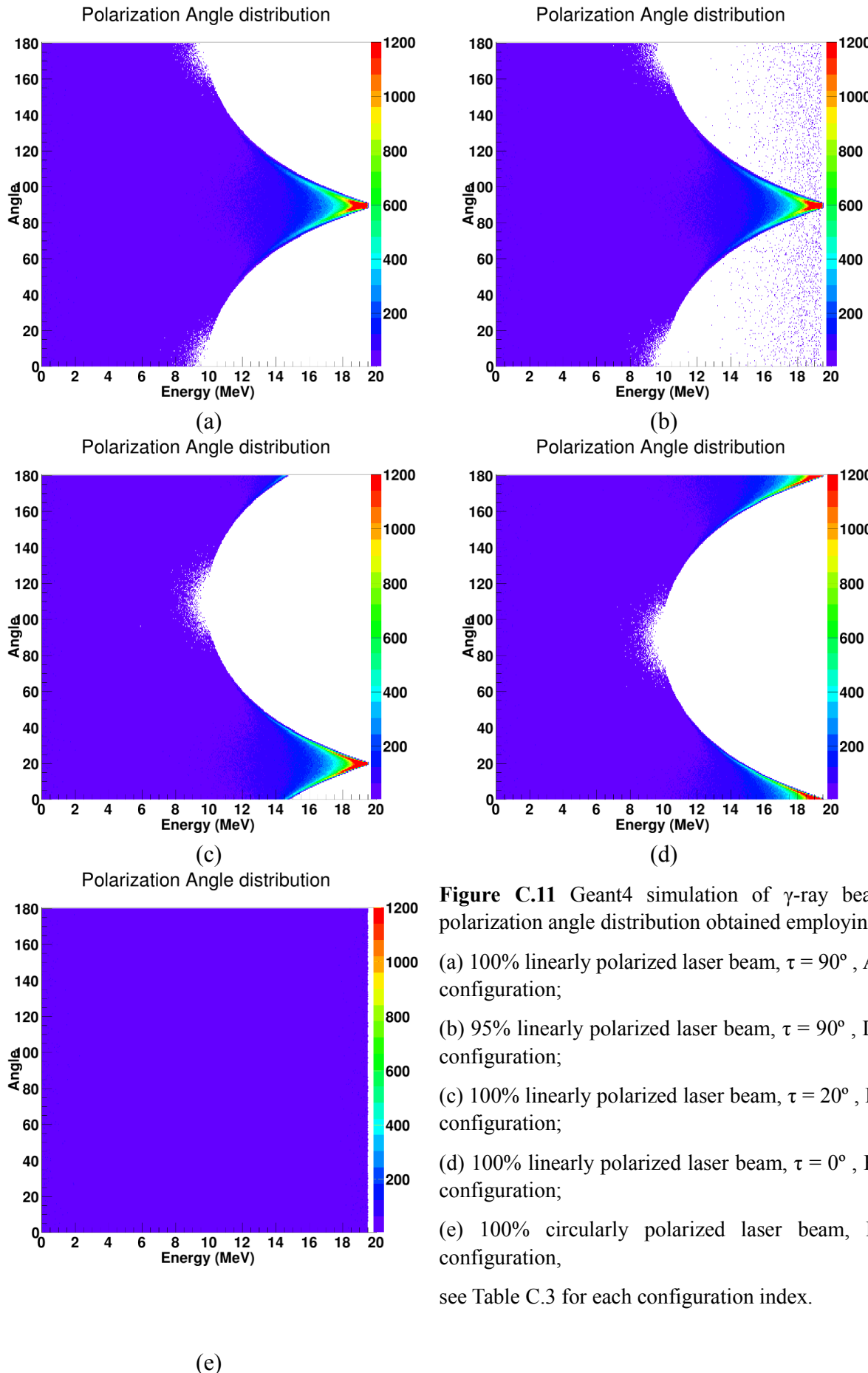


Figure C.11 Geant4 simulation of γ -ray beam polarization angle distribution obtained employing:

- (a) 100% linearly polarized laser beam, $\tau = 90^\circ$, A1 configuration;
- (b) 95% linearly polarized laser beam, $\tau = 90^\circ$, D1 configuration;
- (c) 100% linearly polarized laser beam, $\tau = 20^\circ$, E1 configuration;
- (d) 100% linearly polarized laser beam, $\tau = 0^\circ$, B1 configuration;
- (e) 100% circularly polarized laser beam, F1 configuration,

see Table C.3 for each configuration index.

As an example, Geant4 simulations for a γ -ray beam produced by employing a laser beam characterized by a mixed state of polarization: 50% linearly polarized, $\tau = 20^\circ$ and 30% circularly polarized are presented in the following section. The transverse energy profile, the electron and laser beam phase-space distributions, the Stokes parameters distributions and the polarization angle distribution are represented in Figures C.12 – C.16.

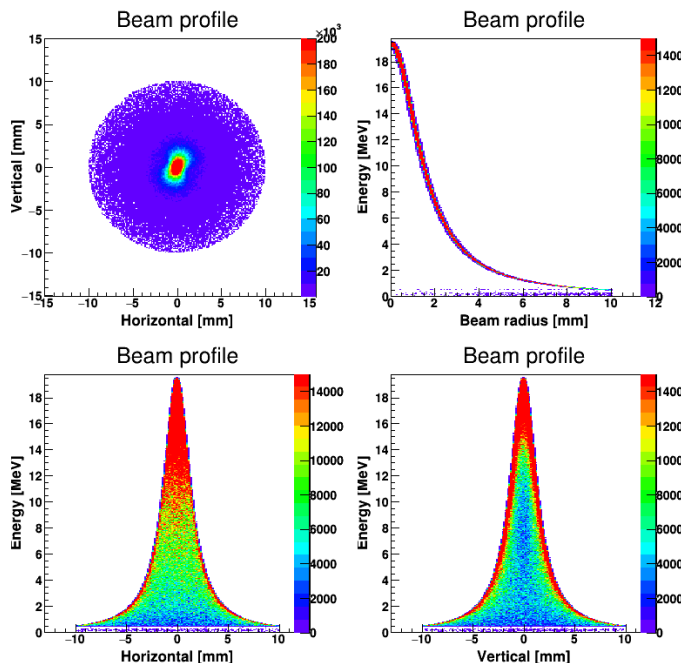


Figure C.12 Geant4 simulation of the transverse energy profile of a 19.557 MeV maximum energy γ -ray beam produced using a laser beam:

50% linearly polarized, $\tau = 20^\circ$;

30% circularly polarized,

corresponding to the G1 scenario listed in Table C.3. The energy profile was investigated at 2.3 meters from the interaction point.

Upper left: γ -ray beam intensity profile.

Upper right: γ -ray beam energy distribution versus beam radius.

Lower left: γ -ray beam energy distribution on the horizontal beam axis.

Lower right: γ -ray beam energy distribution on the vertical beam axis.

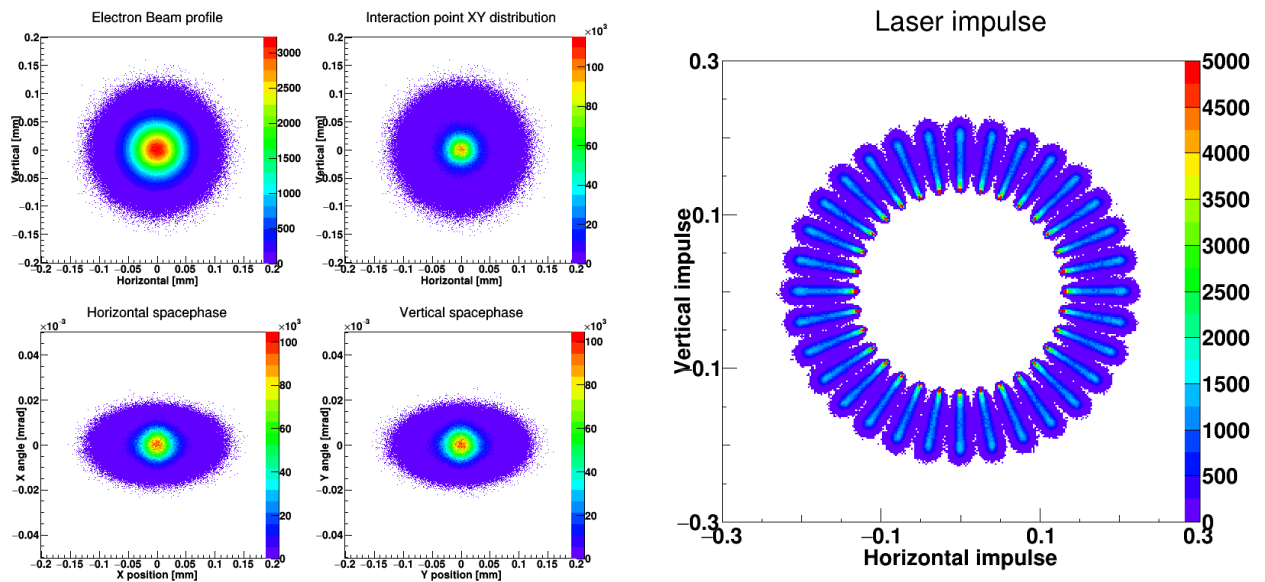


Figure C.13 Transverse electron beam intensity profile (upper left), Interaction point transverse intensity distribution (upper right), Horizontal (lower left) and vertical (lower right) phase-space of

Figure C.14 Transverse laser beam impulse intensity profile. Geant4 produced employing a laser beam: **50% linearly polarized, $\tau = 20^\circ$ and 30% circularly polarized**, (G1 scenario, see Table

electrons in the interaction point. Geant4 simulations produced employing a laser beam: **50% linearly polarized, $\tau = 20^\circ$ and 30% circularly polarized,** (G1 scenario, see Table C.3).

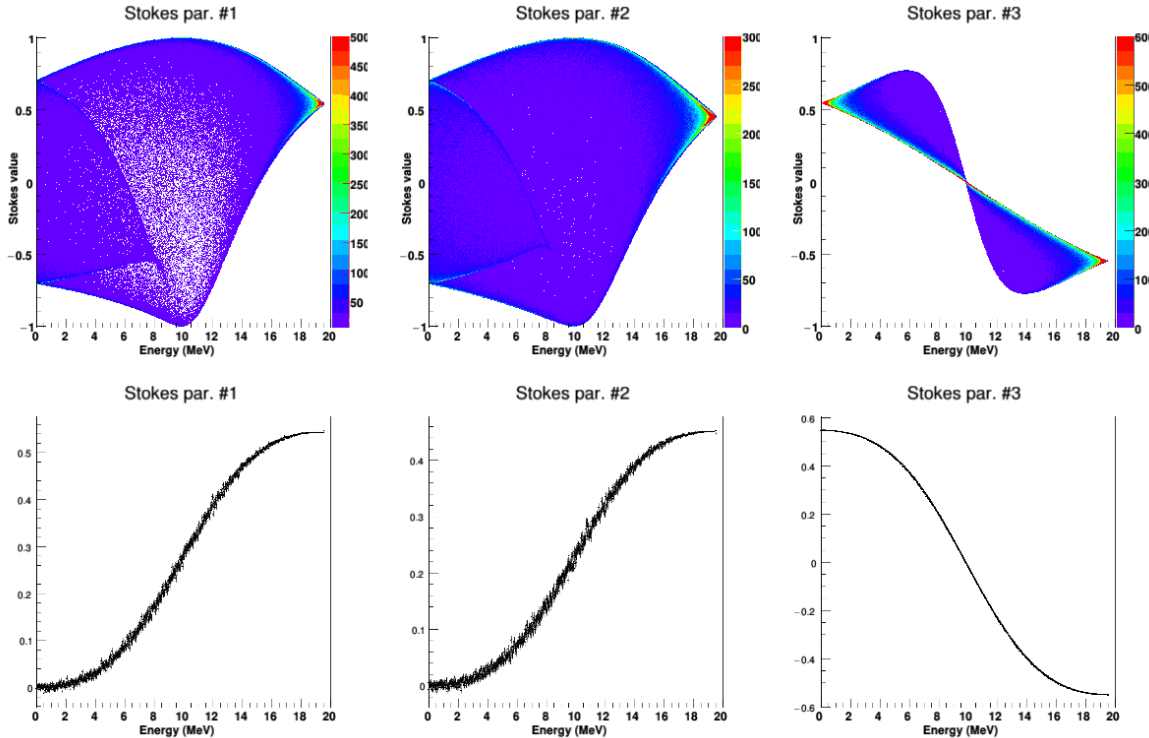


Figure C.15 Geant4 simulation of distribution of γ -ray beam Stokes parameters versus energy. The simulation was produced employing a laser beam: **50% linearly polarized, $\tau = 20^\circ$ and 30% circularly polarized,** (G1 scenario, see Table C.3).

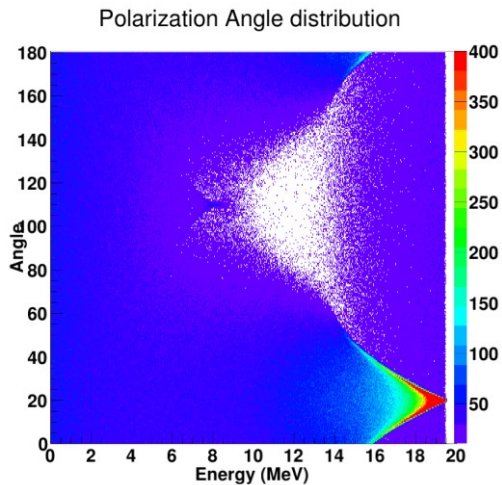


Figure C.16 Geant4 simulation of γ -ray beam polarization angle distribution obtained employing:
50% linearly polarized, $\tau = 20^\circ$;
30% circularly polarized,
corresponding to the G1 scenario listed in Table C.3.

Characterization of ELI-NP LCS γ -ray source – After collimator

The energy and intensity profiles of γ -ray beams after collimation can also be provided by the Geant4 simulation code. Here we present the results for γ -ray beams collimated using the main γ -ray beam collimator to be installed at ELI-NP with a fixed 0.5 mm aperture. Details

about the implementation of the ELI-NP γ -ray beam collimator are given later in this section. A monitor detector was placed in beam in the experimental hall E8, in the center of the multi-detector array in the position where the target will be placed during experiments. Thus, we will present here Geant4 simulations on the energy and intensity profile of the γ -ray beam incident on targets to be used in the GANT experiments.

	A2	B2	C2	D2	E2
ϵ_n [mm×mrad]	0.2	0.6	0.2	0.2	0.6
ΔE [%]	0.04	0.1	0.04	0.1	0.04
σ [μm]	30	15	15	30	30

Table C.4 Electron beam normalized emittance (ϵ_n), central energy spread (ΔE) and electron beam spot size at focal point (σ) used as input parameters for Geant4 simulations on energy and intensity profiles of LCS γ -ray beams incident on a monitor detector placed in beam in the center of the neutron – gamma multi-detector array.

The energy spectra of the γ -ray beams incident on the detector are shown in Figure C.17. The 19.557 MeV maximum energy γ -ray beams were produced using the lower and upper limits of the expected electron beam normalized emittance, central energy spread and transverse beam size at focal point values, which are listed in Table C.4. For comparison, a typical NewSUBARU LCS γ -ray beam energy spectrum is presented. The NewSUBARU beam was obtained using typical electron and laser beam input parameters by placing a monitor detector in the GACKO hutch target position. The difference between the maximum energy of the ELI-NP and of the NewSUBARU simulated γ -ray beams is given by the fact that at NewSUBARU the laser beam is sent head-on against the electrons while at ELI-NP there is a $\theta = 7.5^\circ$ between the laser and the electron beam axes.

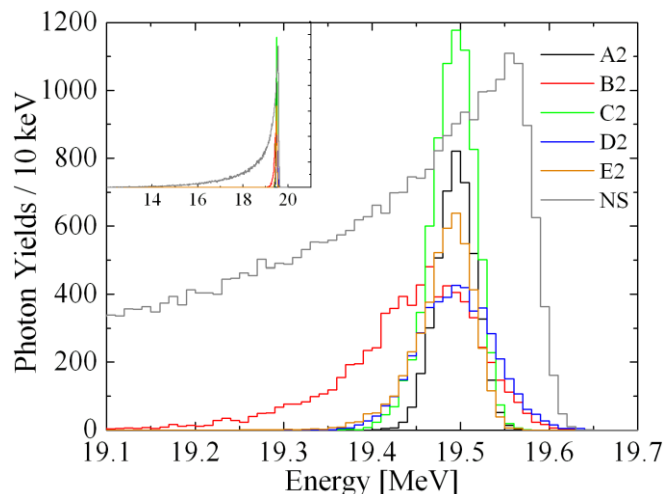


Figure C.17 Geant4 simulations for energy spectra of incident LCS γ -ray beams on a monitor detector placed in beam in the E8 experimental hall. The input parameters for the electron beam emittance, beam spot size at focal point and central energy spread are listed in Table C.4.

The grey line, NS, represents a typical energy spectra for a γ -ray beam produced at NewSUBARU.

Transverse energy and intensity profiles of the collimated γ -ray beams represented above are also provided by the Geant4 code. The γ -ray beam transverse intensity profile, energy distribution versus beam radius, horizontal and vertical beam axes are shown in Figure C.18. Figure C.19 represents the γ -ray beams average energy and the intensity versus beam radius incident on the monitor detector placed in the E8 experimental hall.

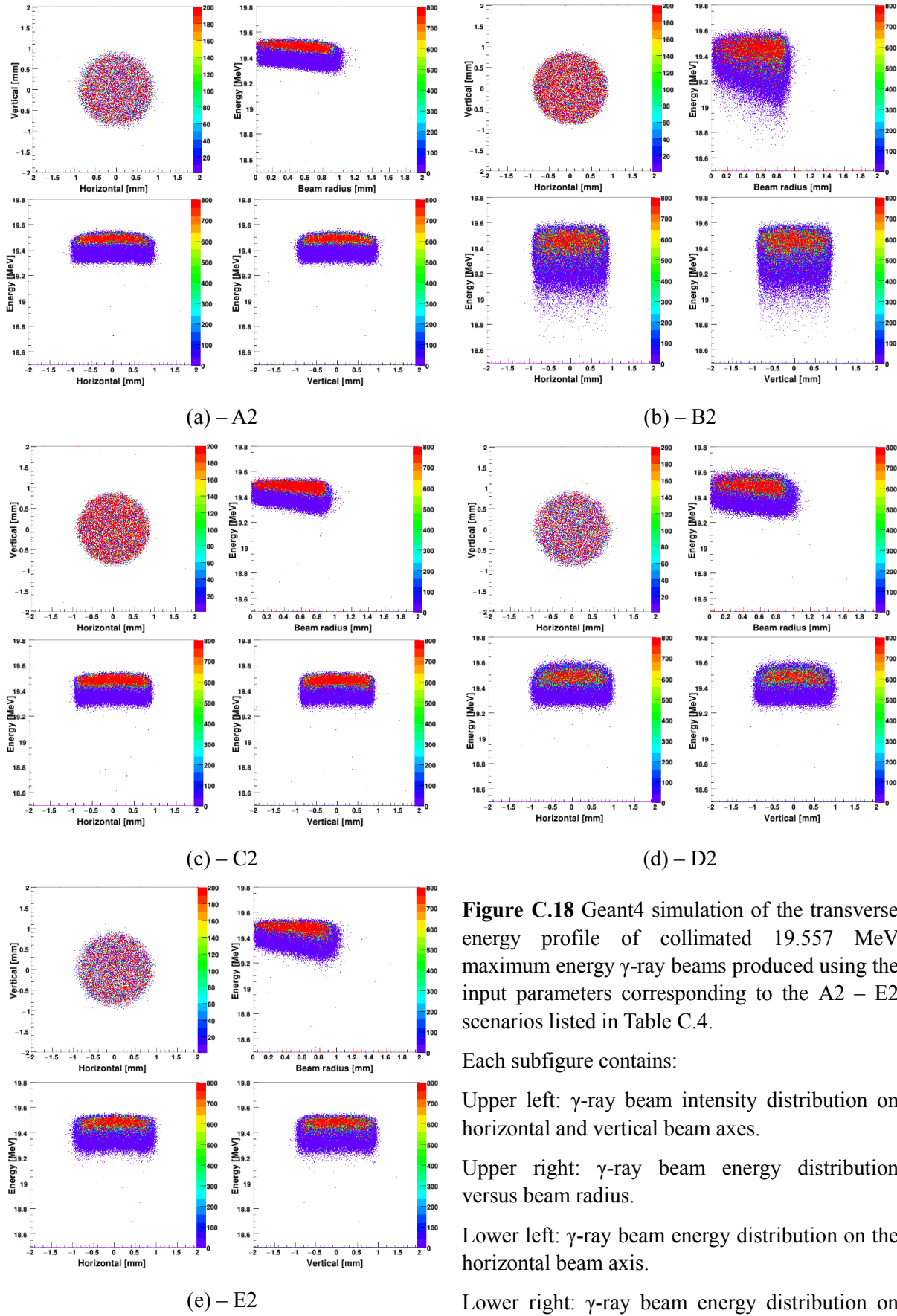


Figure C.18 Geant4 simulation of the transverse energy profile of collimated 19.557 MeV maximum energy γ -ray beams produced using the input parameters corresponding to the A2 – E2 scenarios listed in Table C.4.

Each subfigure contains:

Upper left: γ -ray beam intensity distribution on horizontal and vertical beam axes.

Upper right: γ -ray beam energy distribution versus beam radius.

Lower left: γ -ray beam energy distribution on the horizontal beam axis.

Lower right: γ -ray beam energy distribution on the vertical beam axis.

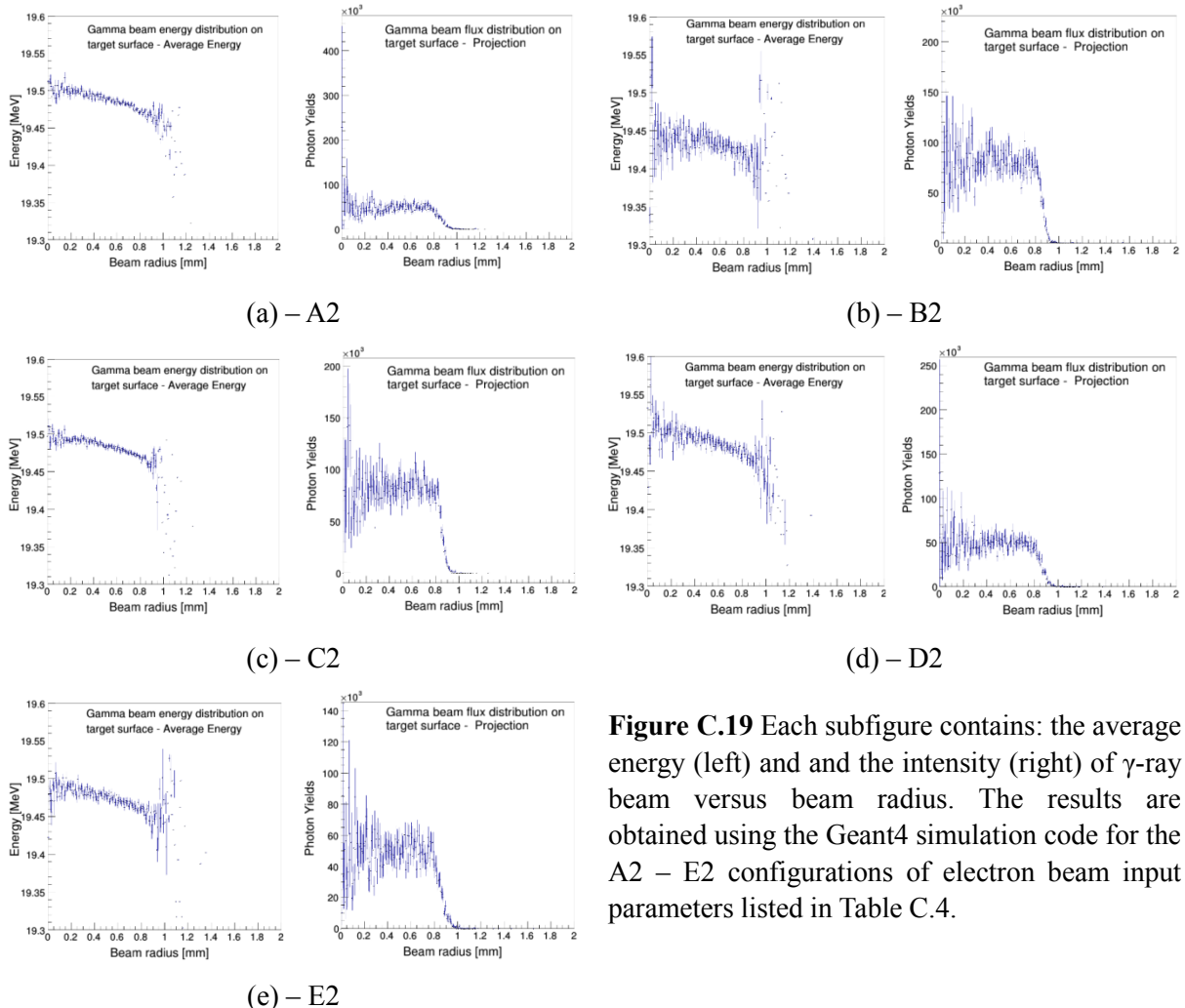


Figure C.19 Each subfigure contains: the average energy (left) and and the intensity (right) of γ -ray beam versus beam radius. The results are obtained using the Geant4 simulation code for the A2 – E2 configurations of electron beam input parameters listed in Table C.4.

C.1.2 IDEAL PENCIL-LIKE GAMMA-RAY SOURCE

Pile-up and γ -ray beam related background studies based on simulations are necessary for developing optimum detection configurations for the ELI-NP experimental conditions created by the LCS γ -ray beam time structure.

Beam induced background and pile-up studies are not affected by the energy and intensity profile of the incident γ -ray beam and can be carried out using a monochromatic gamma ray beam of energy equal to the average energy of the collimated LCS γ -ray beam incident on the target. Also, a very large number of events are required for the pile-up studies, because a single count in the final spectra is produced by summing the contribution of 10^5 events. Therefore, ideal γ -ray sources are implemented in the code for increased computing speed necessary for detection efficiency and background studies.

The ideal pencil-like γ -ray source placed in the laser – electron interaction point emits monochromatic γ -rays along the electron beam axis.

C.1.3 4 π NEUTRON GENERATOR

A neutron point source located in the center of the detection array from the E8 experimental hall was implemented in the code for simulations of:

- neutron detection efficiency;
- neutron anisotropy measurements;
- pile-up effects in detectors;
- sensitivity tests for neutron multipolarity measurements.

The source can emit neutrons either monochromatically or by a Weisskopf-Ewing neutron spectrum given by:

$$p(E) = \frac{1}{T^2} E \times \exp\left(-\frac{E}{T}\right),$$

where E and T , both of them expressed in MeV, represent the neutron energy and a temperature typical for neutron evaporation, respectively.

The neutrons can be generated from the source isotropically or by a given angular distribution function, such as the angular distribution function of p- wave photoneutrons emitted from the target.

Defining the linear polarization by the direction of the electric component of the γ -ray photons (γ -ray beam x axis), the angular distribution for p-wave photoneutrons is expressed by:

$$W(\theta, \varphi) = \frac{3}{8\pi} [\sin^2 \theta (1 + 2 \cos \varphi)],$$

where θ stands for the polar angle for photoneutron emission with respect to the beam direction (z axis), while φ stands for the azimuthal angle with respect to the x axis. A graphic representation of the angular distribution is displayed in Figure C.20, where the 100% linearly polarized γ -ray beam that hits the target is moving along the z axis towards positive values.

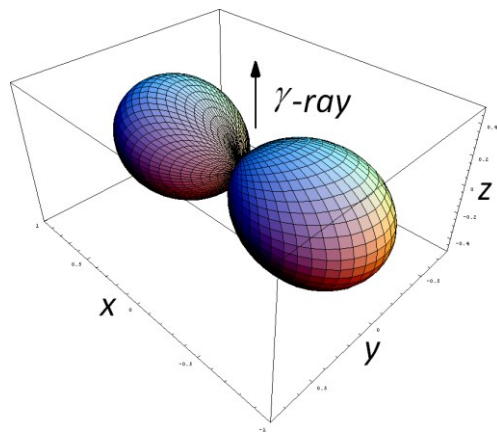


Figure C.20 Angular distribution for p-wave neutrons evaporation using 100% linearly polarized γ -ray beams. The γ -ray is moving along the z axis towards positive values.

In the case of circularly polarized γ -ray beams with the electric component distributed in the x - y plane, the angular distribution is given by

$$W(\theta, \varphi) = \frac{3}{8\pi} \sin^2 \theta.$$

Figures C.21.a-d show neutron angular emission distributions in the $(\sin(\theta), \varphi)$ coordinate system for various neutron multipolarity values and γ -ray beam polarization states and the corresponding probability distributions for neutrons to hit mixed scintillation arrays detectors.

The effect of the surrounding walls and materials give a contribution to the scattering of neutrons and thus the background can easily be identified in the figures.

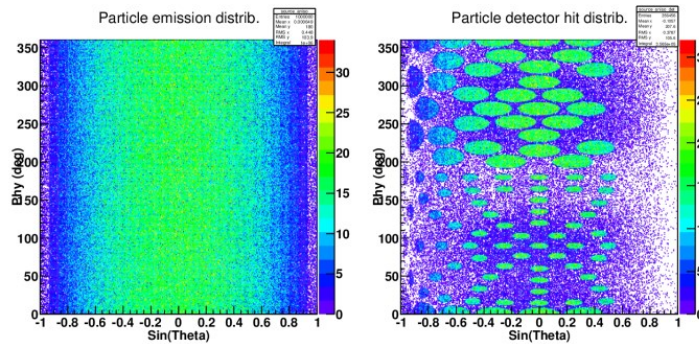
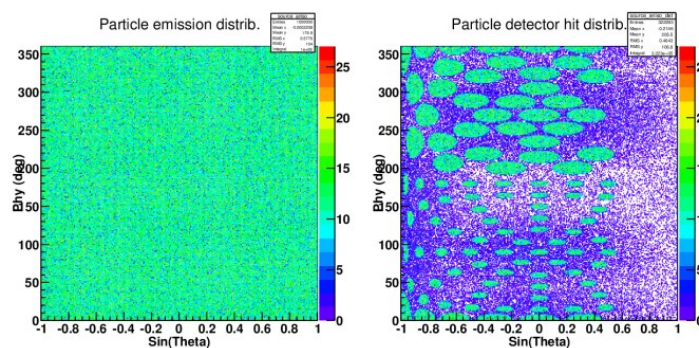
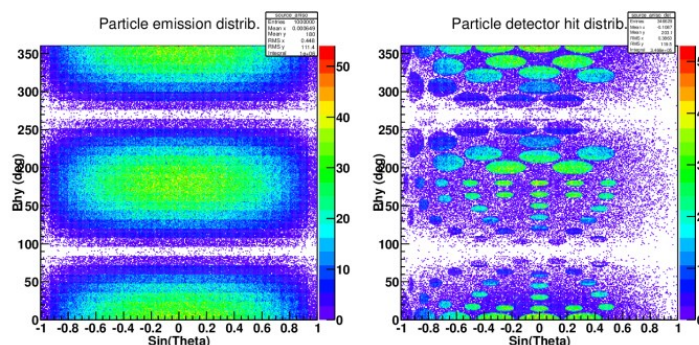


Figure C.21 For each subfigure: (left) neutron angular emission distribution in the $(\sin(\theta), \phi)$ coordinate system for various neutron multipolarity values and γ -ray beam polarization states; (right) corresponding probability distribution for neutrons to hit mixed scintillation arrays detectors. The neutron multipolarity and the state of γ -ray beam polarization are given in each subfigure.

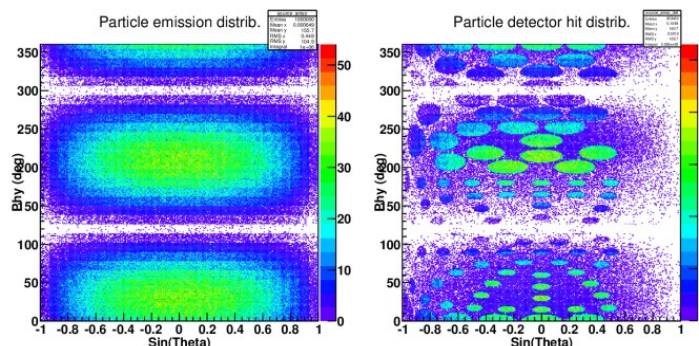
(a) p-wave neutrons, circularly polarized beam.



(b) Isotropic s-wave neutron emission.



(c) p-wave neutrons, linearly polarized beam, $\tau = 0$ deg.



(d) p-wave neutrons, linearly polarized beam, $\tau = 30$ deg.

C.1.4 4 π GAMMA RAY GENERATOR

A γ -ray point source located in the center of the detection array was implemented in the code for simulations of:

- γ -ray detection efficiency;
- the polarization sensitivity (or resolving power) of experimental setups;
- pile-up effects in detectors;
- sensitivity tests for γ -ray multipolarity and electric/magnetic character measurements.

The angular distribution function for E1 and M1 transitions from a nuclear state excited using 100% linearly polarized γ -rays is implemented in the simulation code as:

$$W(\theta, \varphi) = 1 + \frac{1}{2} \left[P_2(\cos \theta) + \frac{1}{2} \pi \cos(2\varphi) P_2^{(2)}(\cos \theta) \right],$$

where π denotes the parity of the excited state, and θ and φ denote the polar and azimuthal angle, respectively. The terms $P_2(\cos \theta)$ and $P_2^{(2)}(\cos \theta)$ denote the second order ordinary and unnormalized associated Legendre polynomials. A graphic representation of the angular distribution is displayed in Figure C.22, where the 100% linearly polarized γ -ray beam that hits the target is moving along the z axis towards positive values.

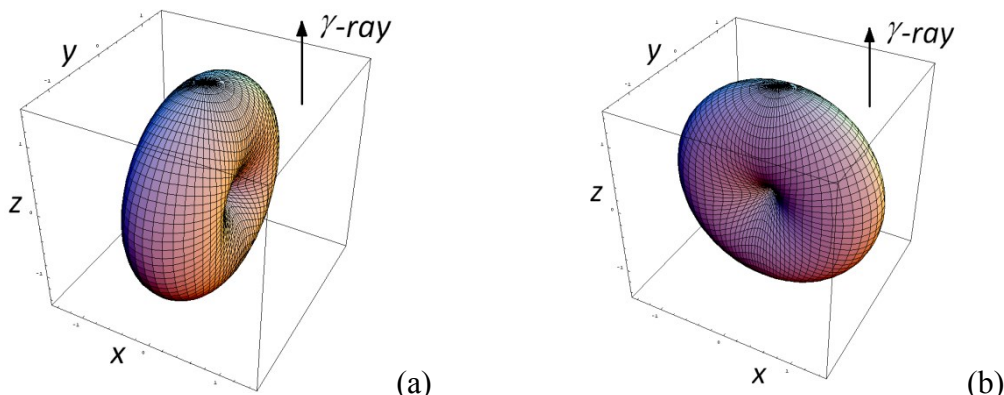


Figure C.22 Angular distribution functions for (a) E1 and (b) M1 transitions from a nuclear state excited using 100% linearly polarized γ -rays. The γ -ray is moving along the z axis towards positive values.

The angular distribution for excitation using circularly polarized γ -rays is implemented as:

$$W_c(\theta) = 1 + \frac{1}{2} P_2(\cos \theta).$$

Figure C.23 shows plots of the γ -ray angular emission distribution in the $(\sin(\theta), \varphi)$ coordinate system for various transition multipolarity values and γ -ray beam polarization states. This system of coordinates was chosen so that the isotropic distribution to coincide with the uniform distribution. Also the corresponding probability distribution for a γ -ray to hit the mixed scintillation arrays detectors is represented.

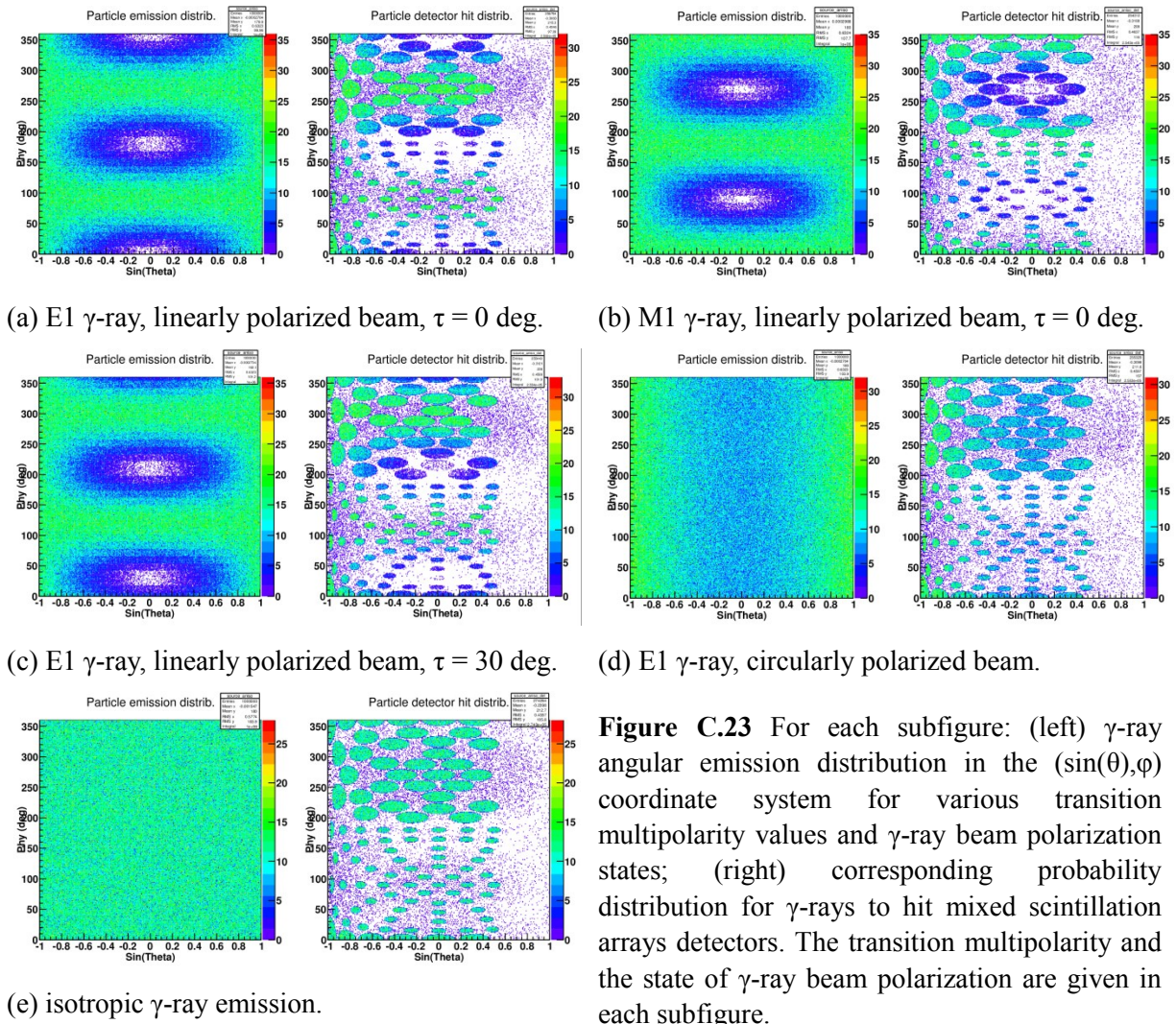


Figure C.23 For each subfigure: (left) γ -ray angular emission distribution in the $(\sin(\theta), \phi)$ coordinate system for various transition multipolarity values and γ -ray beam polarization states; (right) corresponding probability distribution for γ -rays to hit mixed scintillation arrays detectors. The transition multipolarity and the state of γ -ray beam polarization are given in each subfigure.

C.1.5 POSSIBLE CONFIGURATIONS OF RADIATION SOURCES

Depending on the requirements of the study, different source configurations can be employed using the Geant4 simulation code. An input file for the source configuration is described in Table C.5. The user must first chose between using the realistic Laser – Compton γ -ray source or the ideal gamma and neutron point sources. If the LCS γ -ray source is chosen, the rest of the input file is disregarded and the input parameters for the electron and laser beam are read from a different input file described in Table C.2. If the ideal sources are employed, the probabilities for gamma and neutron emission from the 4π point sources placed in the center of the array must be given separately. The probability for gamma emission from the pencil-like source placed in the laser – electron interaction point, p_γ , is computed as $p_\gamma = 100\% - p_n^{4\pi} - p_\gamma^{4\pi}$, where $p_n^{4\pi}$ and $p_\gamma^{4\pi}$ represent the probabilities for neutron and gamma emission from the 4π sources, respectively.

Input value	Unit	Comments
1	–	Switch: 1 = consider Laser – Compton scattering γ -ray source. 0 = consider ideal gamma and neutron sources.
90.	deg	$\tau \in [0,90]$ → consider 100% linearly polarized γ -rays emitted from the pencil-like source with polarization plane angle of τ ; $\tau < 0$ → consider 100% circularly polarized γ -rays emitted from the pencil-like source.
30.	%	Probability for γ -ray emission from the point source located in the center of the detection array
20.	%	Probability for neutron emission from the point source located in the center of the detection array
18.	MeV	Energy of γ -rays emitted from the 4π point source and from the pencil-like source placed in the laser-electron interaction point.
1	MeV	Neutron energy / Neutron evaporation temperature
0	–	Switch: 0 = isotropic emission of γ -rays from the 4π source. 1 = E1 anisotropic γ -rays emission from the 4π source. 2 = M1 anisotropic γ -rays emission from the 4π source.
0	–	Switch: 0 = isotropic emission of s-wave neutrons. 1 = anisotropic emission of p-wave neutrons.
0	–	Switch: 0 = monochromatic neutron point source. 1 = Weisskopf-Ewing neutron spectrum point source.

Table C.5 Geant4 code input file for configuration of radiation sources. The each input parameters is explained in Column 3.

The energy of the γ -ray emitted from the 4π source and from the pencil-like source placed in the laser-electron interaction point must be given as input, along with the type of emission, isotropic or by E1/M1 anisotropy.

Also the neutron type of emission spectra must be given as input: monochromatic or by a Weisskopf-Ewing spectrum. In the case of monochromatic emission, the neutron energy must be given as input, while for a Weisskopf-Ewing spectrum the neutron evaporation temperature must be provided by the user. The type of isotropic or anisotropic emission of s-wave and p-wave neutrons, respectively, must be given in the input file.

The list of all possible configurations of radiation sources implemented in the Geant4 simulation code is given in Table C.6 along with the main applications characteristic to each configuration.

Nb.	Sources	Observations
1.	LCS γ -ray	<ul style="list-style-type: none"> - γ-ray beam energy spectra incident on a monitor detector; - transverse energy and intensity beam profile; - type and degree of polarization; - collimator configuration and misalignment studies.
2.	Pencil-like γ -ray	<ul style="list-style-type: none"> - beam induced background studies; - pile-up studies.
3.	4π neutron	<ul style="list-style-type: none"> - neutron detection efficiency; - neutron anisotropy measurements; - pile-up effects in detectors; - sensitivity tests for neutron multipolarity measurements.
4.	4π γ -ray	<ul style="list-style-type: none"> - γ-ray detection efficiency; - the polarization sensitivity (or resolving power) of experimental setups; - pile-up effects in detectors; - sensitivity tests for γ-ray multipolarity and electric/magnetic character measurements.
5.	Pencil-like γ -ray + 4π γ -ray + 4π neutron	<ul style="list-style-type: none"> - sensitivity tests for detecting γ-ray induced radiation by photoneutron and (γ, γ) reactions in the presence of strong beam induced background. For a given energy and target thickness, the emission probabilities from the 4π neutron and γ-ray sources can be given accordingly to the nuclear reactions cross sections.
6.	4π γ -ray + 4π neutron	<ul style="list-style-type: none"> - investigation of the ideal case composed only of γ-ray induced radiation by photoneutron and (γ, γ) reactions. For a given energy, the emission probabilities from the 4π neutron and γ-ray sources can be given accordingly to the (γ, n) and (γ, γ) cross sections.
7.	4π neutron + pencil-like γ -ray	<ul style="list-style-type: none"> - sensitivity tests for detecting photo-neutrons in the presence of beam induced background. For a given energy and target thickness, the emission probabilities from the 4π neutron source can be given accordingly to the (γ, n) cross section.
8.	4π γ -ray + pencil-like γ -ray	<ul style="list-style-type: none"> - sensitivity tests for identifying the (γ, γ) reaction channel in the presence of beam induced background. For a given energy and target thickness, the emission probability from the 4π γ-ray source can be given accordingly to the (γ, γ) cross section.

Table C.6 Possible configurations of radiation sources implemented in the Geant4 simulation code.